# Supporting Information

Lin Zhu,[#a] Pu Gao, [#a] Jing Du, [#b] Yan Shen, [a] Yan Feng, [*c] Mingzai Wu, [*a] Yanjun Ding, [*a] Manzhou Zhu[c]

[a] School of Materials Science and Engineering, Anhui University, Hefei 230601, China.

[b] Testing and Analysis Center, Hebei Normal University, Shijiazhuang 050024, China.

[c] Department of Chemistry and Centre for Atomic Engineering of Advanced Materials, Anhui Province Key Laboratory of Chemistry for Inorganic/Organic Hybrid Functionalized Materials, Key Laboratory of Structure and Functional Regulation of Hybrid Materials, Anhui University, Ministry of Education, Anhui University, Anhui University, Hefei 230601, China.

## Experimental Procedures

***1.1. Materials.*** All reagents are commercially available and used directly without further purification, including CuCl (98%), 4-methylbenzenethiolate (98%), 4-isopropylbenzenethiol (95%), 4-tert-butylbenzenethiol (98%), tetraoctylammonium bromide (TOAB, 98%), triphenylphosphine (TPP, 98%), sodium borohydride (99.99%), chloroform (HPLC grade, ≥ 99.9%), methanol (HPLC grade, ≥ 99.9%), *n*-hexane (HPLC grade, ≥ 99.9%). $Me_2SAuCl$, Au(TPP)Cl and $[Cu_{23}(SC_6H_4\text{-}R)_{18}(TPP)_6](SbF_6)$ were prepared according to literature methods. [1-3]

***1.2. Synthesis of the $[AuCu_{14}(SC_6H_4\text{-}CH_3)_{12}(TPP)_6](SbF_6)$ cluster.***
The whole reaction process was carried out at room temperature. 5 mg of the $[Cu_{23}(SC_6H_4\text{-}CH_3)_{18}(TPP)_6](SbF_6)$ nanocluster was firstly dissolved in 2 mL of $CH_2Cl_2$ under stirring.Then, Au(TPP)Cl (0.5 mg) was added to the above solution. After irradiated at 365 nm for 30 seconds, the solution gradually changed from light yellow to red, accompanied by a bright red light. The organic solution was evaporated and washed several times with methanol. Finally, red crystals were obtained by liquid diffusion of *n*-hexane into a $CH_2Cl_2$ solution of the nanocluster for three days with a ~60% yield (Cu atom basis). ESI-MS ($[AuCu_{14}(SC_6H_4\text{-}CH_3)_{12}(TPP)_5]^+$): m/z = 3876.75 (cald. 3876.75).

***1.3. Synthesis of the $[AuCu_{14}(SC_6H_4\text{-}CH(CH_3)_2)_{12}(TPP)_6](SbF_6)$ cluster.***
The whole reaction process was carried out at room temperature. 5 mg of the $[Cu_{23}(SC_6H_4\text{-}CH(CH_3)_2)_{18}(TPP)_6](SbF_6)$ nanocluster was firstly dissolved in 2 mL of $CH_2Cl_2$ under stirring.Then, Au(TPP)Cl (0.5 mg) was added to the above solution. After irradiated at 365 nm for 30 seconds, the solution gradually changed from light yellow to red, accompanied by a bright red light. The organic solution was evaporated and washed several times with methanol. Finally, red crystals of were obtained by liquid diffusion of *n*-hexane into a $CH_2Cl_2$ solution of the nanocluster for three days with a ~25% yield (Cu atom basis). ESI-MS ($[AuCu_{14}(SC_6H_4\text{-}CH(CH_3)_2)_{12}(TPP)_5]^+$): m/z = 4213.15 (cald. 4212.75).

***1.4. Synthesis of the $[AuCu_{14}(SC_6H_4\text{-}C(CH_3)_3)_{12}(TPP)_6](SbF_6)$ cluster.***
The whole reaction process was carried out at room temperature. 5 mg of the $[Cu_{23}(SC_6H_4\text{-}C(CH_3)_3)_{18}(TPP)_6](SbF_6)$ nanocluster was firstly dissolved in 2 mL of $CH_2Cl_2$ under stirring.Then, Au(TPP)Cl (0.5 mg) was added to the above solution. After irradiated at 365 nm for 30 seconds, the solution gradually changed from light yellow to red, accompanied by a bright red light. The organic solution was evaporated and washed several times with methanol. Finally, red crystals of were obtained by liquid diffusion of *n*-hexane into a $CH_2Cl_2$ solution of the nanocluster for three days with a ~38% yield (Cu atom basis).. ESI-MS ($[AuCu_{14}(SC_6H_4\text{-}C(CH_3)_3)_{12}(TPP)_4]^+$): m/z = 4119.19 (cald. 4118.46).

***1.5. Titration experiments.***
1.7 mg of $AgNO_3$ was dissolved in 5 mL of methanol under stirring to obtain a homogeneous $AgNO_3$ solution with a concentration of 0.34 mg/mL (~2.0 mM). Then, 3 mL of **$AuCu_{14}\text{-}CH(CH_3)_2$** (0.2 mg/mL) solution in $CH_2Cl_2$ was placed in a cuvette to record its initial fluorescence spectrum. After the addition of $AgNO_3$ solution (15 μL, ~10 μM) to the above $CH_2Cl_2$ solution, the cuvette was gently shaked to ensure thorough mixing and record its fluorescence spectrum. This process was repeated sevaral times to obtain fluorescence titration spectra covering the $Ag^+$ concentration range of 0-100 μM. The titration experiments of other metal ions were similar to $Ag^+$ ion.

## Characterization

***2.1. Photoluminescence spectra.*** Photoluminescence spectra were measured using an FL-7000 spectrofluorometer with the same optical density (OD) of ~0.2. Absolute quantum yield (QY) and emission lifetime were measured on the HORIBA FluoroMax-4P.

***2.2. UV-vis absorption spectra.*** UV-visible absorption spectra were recorded on M4 spectrophotometer. Crystals are dissolved in solution.

***2.3. Single Crystal X-ray Diffraction.*** Single crystal X-ray diffraction data were recorded on a Rigaku XtaLAB Synergy-R Diffraction equipped with a digital camera diffractometer comprising a microfocus rotating anode X-ray source (Cu Kα, λ= 1.54178 Å) and an HPC detector [HyPix-6000C] radiation for the crystal structures. The diffraction data were processed during data collection using CrysAlis$^{Pro}$. The structures were solved and refined during data collection with AutoChem. Final structure refinements were performed using SHELXL implemented in Olex2.[4-6] Data collection, structure refinement parameters and crystallographic data for the crystals are given in Table S1.

***2.4. Electrospray ionization (ESI) mass spectrum***. Electrospray ionization mass spectra (ESI-MS) were acquired on a Waters Q-TOF mass spectrometer equipped with a Z-spray source. The samples are dissolved in a mixture solution of $CH_2Cl_2/CH_3OH$ (v:v = 1:1), which is directly infused into the chamber at 20 μL/min with positive mode.

***2.5. X-ray photoelectron spectroscopy (XPS)***. X-ray photoelectron spectroscopy measurements were performed on Thermo ESCALAB 250 equipped with a monochromated Al Kα (1486.8 eV) 150 W X-ray source, 0.5 mm circular spot size, a flood

gun to counter charging effects, and theS3 analysis chamber base pressure lower than $1\times10^{-9}$ mbar; data were collected with FAT = 20 eV. The the sample holder was aluminum plate used during the X-ray Photoelectron Spectroscopy (XPS) analysis.

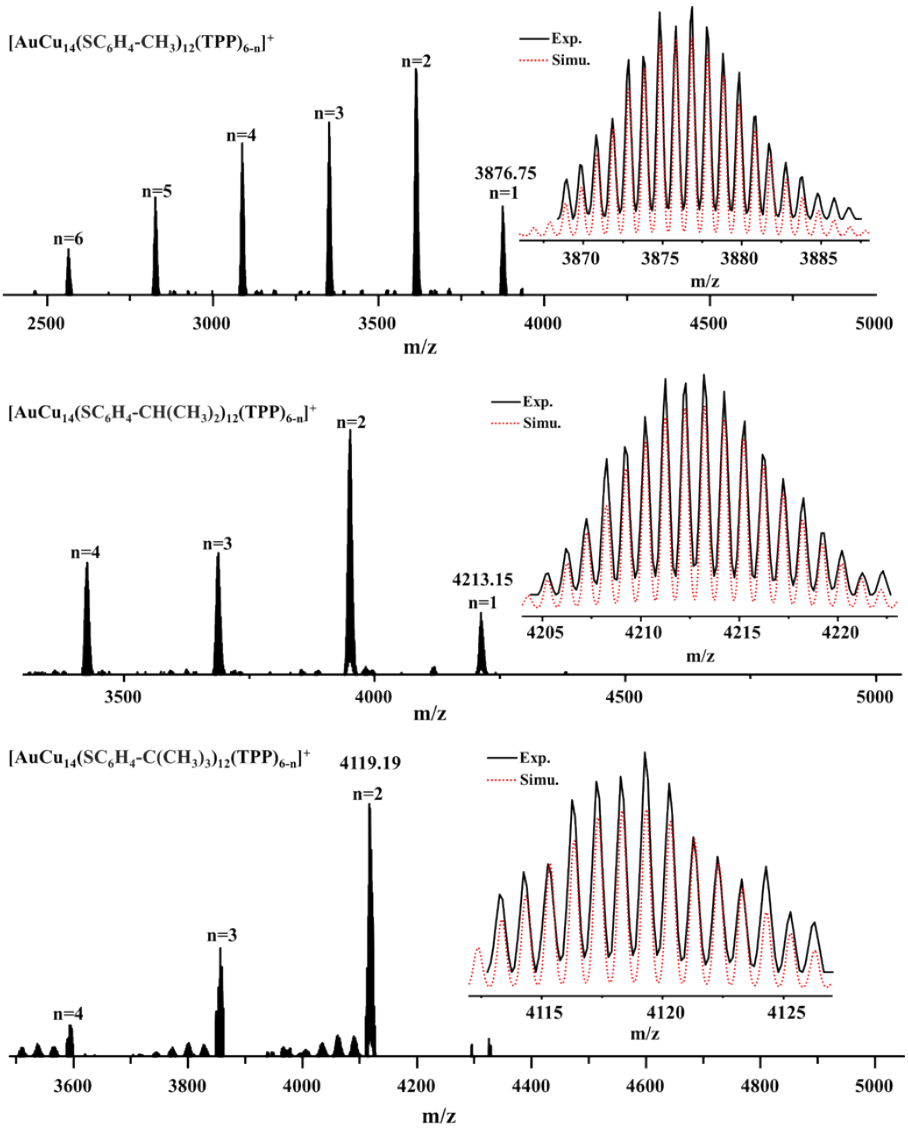


**Figure S1.** Positive-mode ESI mass spectra of **$AuCu_{14}$-$CH_3$**, **$AuCu_{14}$-$CH(CH_3)_2$** and **$AuCu_{14}$-$C(CH_3)_3$**.

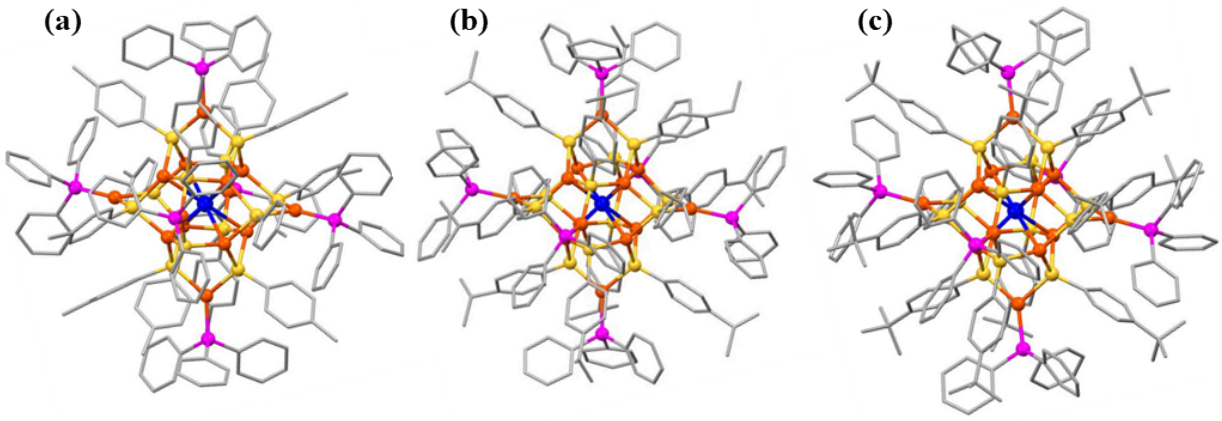


**Figure S2.** The overall structure of the $AuCu_{14}$ cluster shown in ball-and-stick mode: (a) **$AuCu_{14}$-$CH_3$**, (b) **$AuCu_{14}$-$CH(CH_3)_2$** and (c) **$AuCu_{14}$-$C(CH_3)_3$**. Cu orange, Au blue, S yellow, P pink, C gray. H atoms are omitted for clarity.

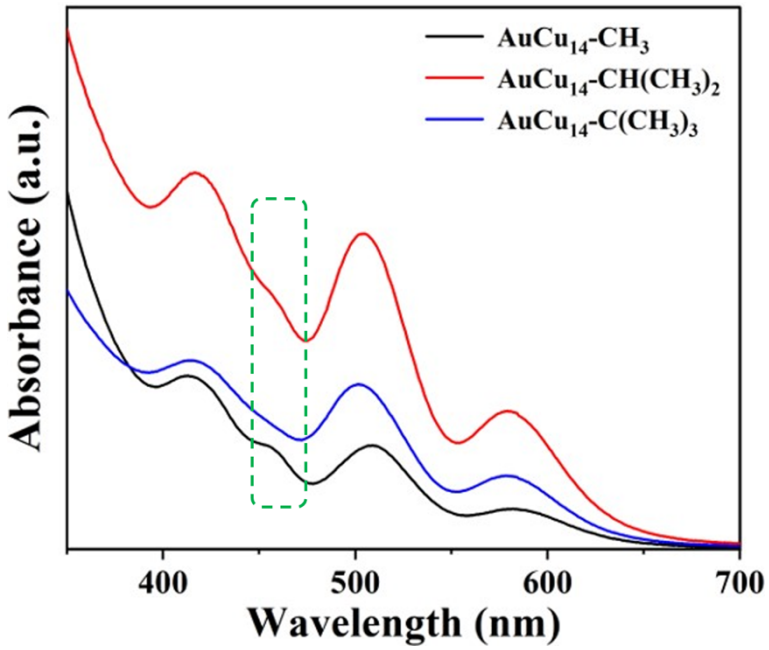


**Figure S3.** UV-vis absorption spectra of **$AuCu_{14}$-$CH_3$**, **$AuCu_{14}$-$CH(CH_3)_2$** and **$AuCu_{14}$-$C(CH_3)_3$** in $CH_2Cl_2$ solution at room temperature.

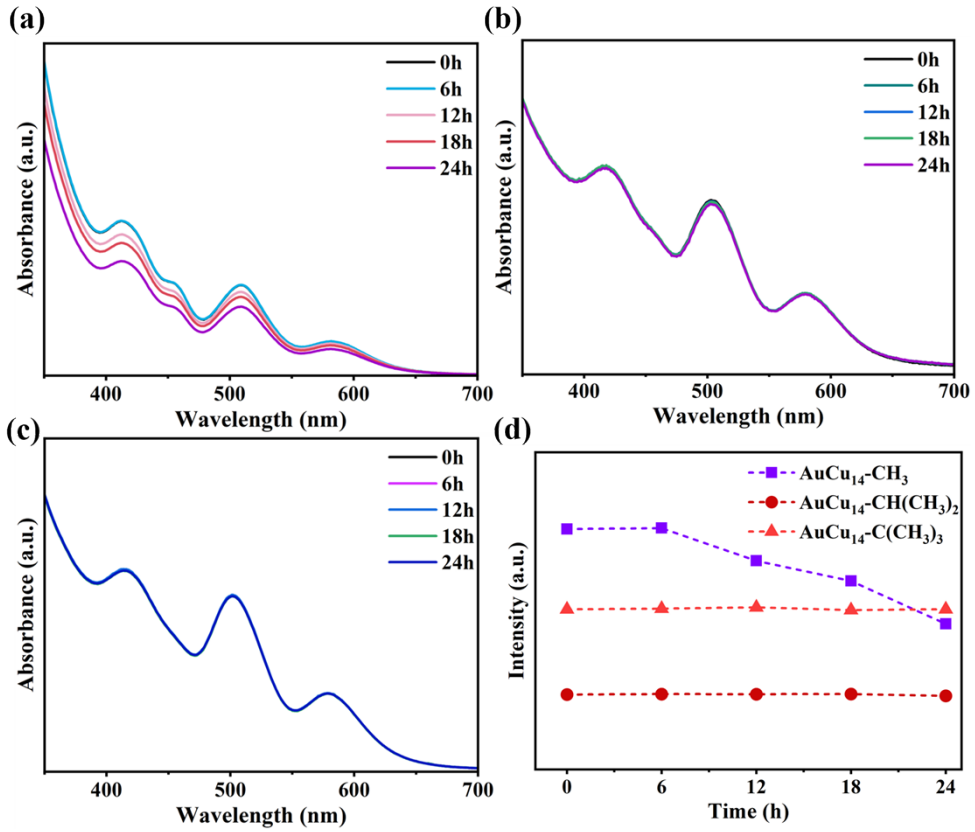


**Figure S4.** The time-dependent UV-vis absorption spectra of (a) **$AuCu_{14}$-$CH_3$**, (b) **$AuCu_{14}$-$CH(CH_3)_2$** and (c) **$AuCu_{14}$-$C(CH_3)_3$** in $CH_2Cl_2$ solution at room temperature. (d) The change of absorption intensity located at 415 nm along with time.

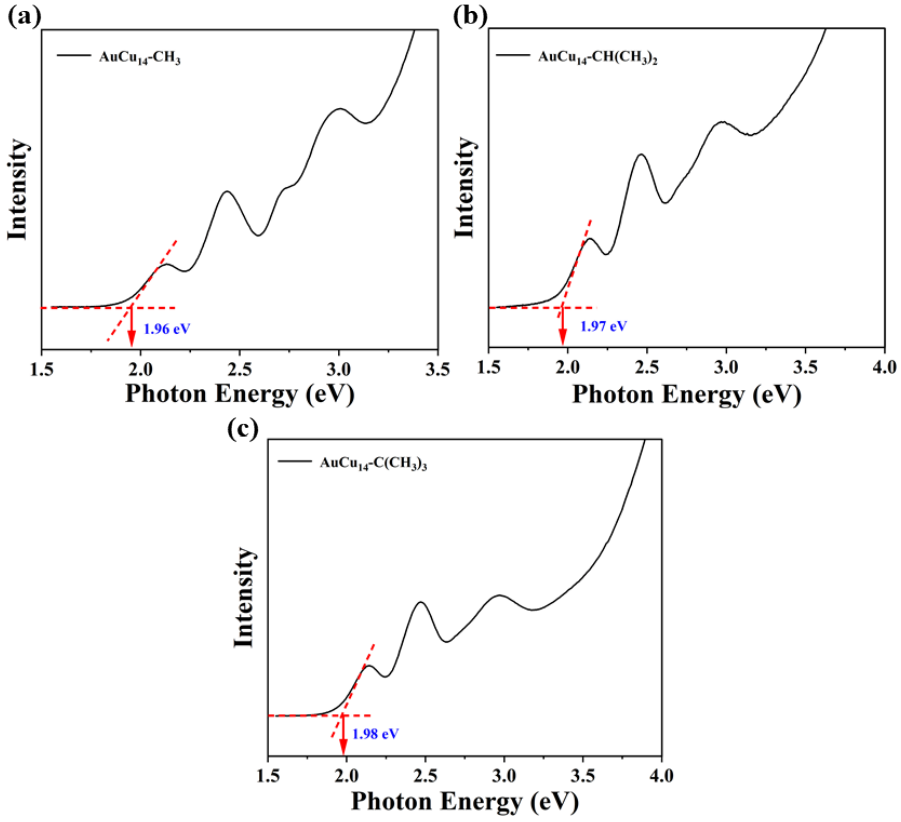


**Figure S5.** Optical gap determination of **$AuCu_{14}$-$CH_3$**, **$AuCu_{14}$-$C(CH_3)_2$** and **$AuCu_{14}$- $C(CH_3)_3$** in $CH_2Cl_2$ solution.

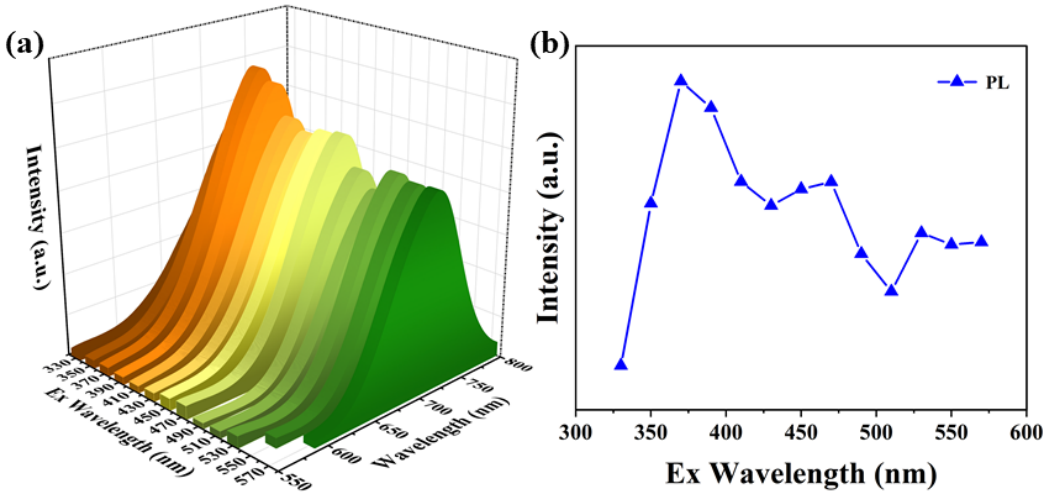


**Figure S6.** The change trends of PL centered at 720 nm of **$AuCu_{14}$-$C(CH_3)_3$** under different excitations in $CH_2Cl_2$.

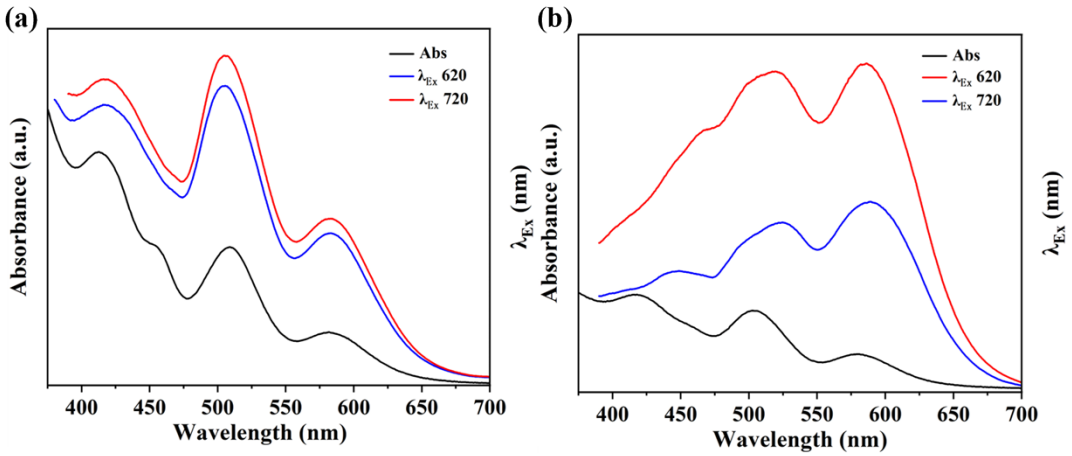


**Figure S7.** The PL excitation spectra and UV-vis absorption spectra of (a) **$AuCu_{14}$-$CH_3$** and (b) **$AuCu_{14}$-$CH(CH_3)_2$** in $CH_2Cl_2$ solution at room temperature.

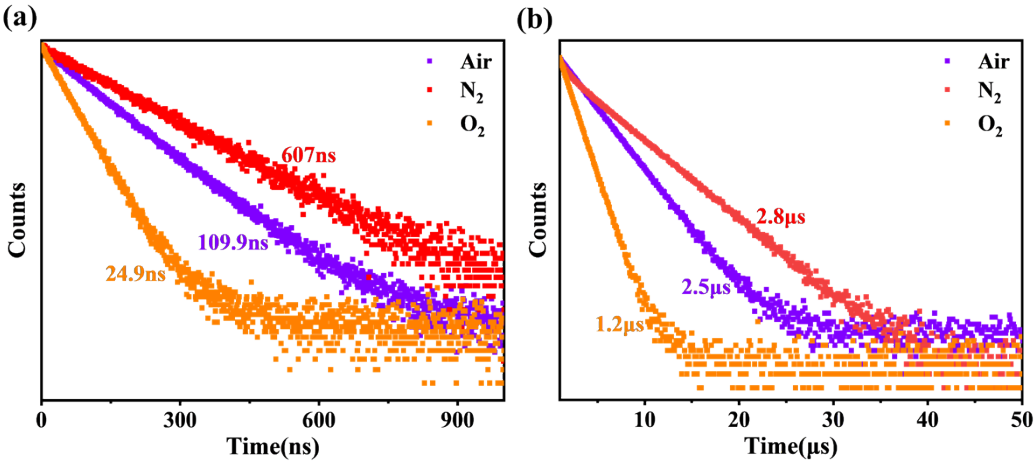


**Figure S8.** (a) The PL I and (b) PL II emission lifetime of **$AuCu_{14}$-$CH_3$** in $CH_2Cl_2$ solution under air, $O_2$ and $N_2$ atmospheres, respectively.

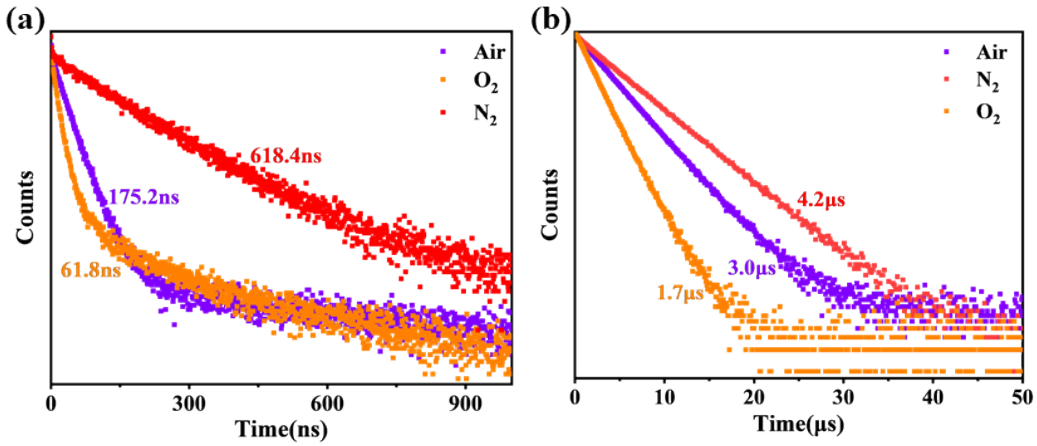


**Figure S9.** (a) The PL I and (b) PL II emission lifetime of **$AuCu_{14}$-$CH(CH_3)_2$** in $CH_2Cl_2$ solution under air, $O_2$ and $N_2$ atmospheres, respectively.

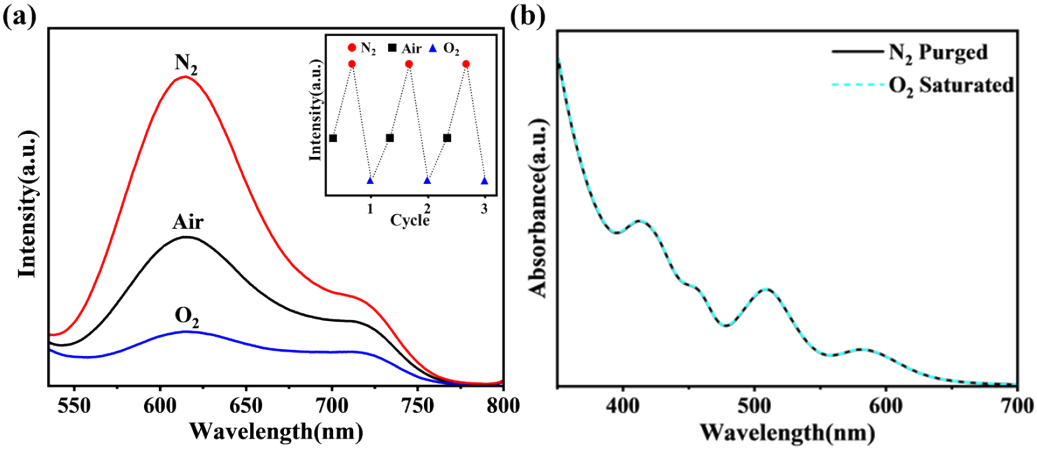


**Figure S10.** (a) Emission spectra of **$AuCu_{14}$-$CH_3$** in $CH_2Cl_2$ solution under air, $O_2$ and $N_2$ atmospheres (inset: the intensity at 620 nm with 3 cycles under different atmospheres). (b) UV-vis spectra of **$AuCu_{14}$-$CH_3$** in $CH_2Cl_2$ solution protected by $N_2$ and $O_2$.

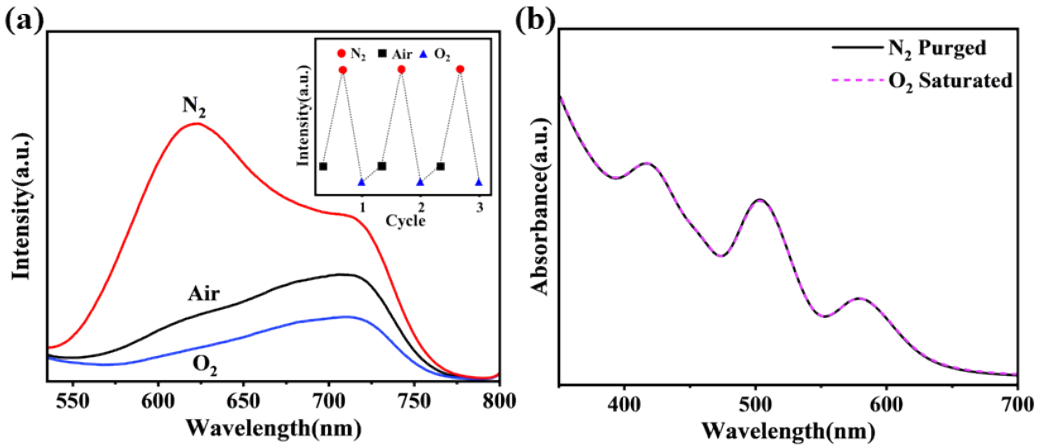


**Figure S11.** (a) Emission spectra of **$AuCu_{14}$-$CH(CH_3)_2$** in $CH_2Cl_2$ solution under air, $O_2$ and $N_2$ atmospheres (inset: the intensity at 620 nm with 3 cycles under different atmospheres). (b) UV-vis spectra of **$AuCu_{14}$-$CH(CH_3)_2$** in $CH_2Cl_2$ solution protected by $N_2$ and $O_2$.

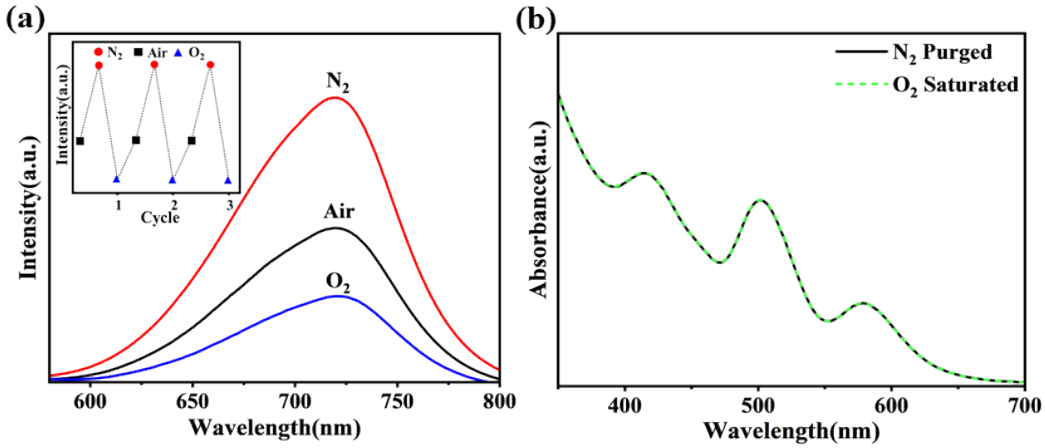


**Figure S12.** (a) Emission spectra of **$AuCu_{14}$-$C(CH_3)_3$** in $CH_2Cl_2$ solution under air, $O_2$ and $N_2$ atmospheres (inset: the intensity at 720 nm with 3 cycles under different atmospheres); (b) UV-vis spectra of **$AuCu_{14}$-$C(CH_3)_3$** in $CH_2Cl_2$ solution protected by $N_2$ and $O_2$.

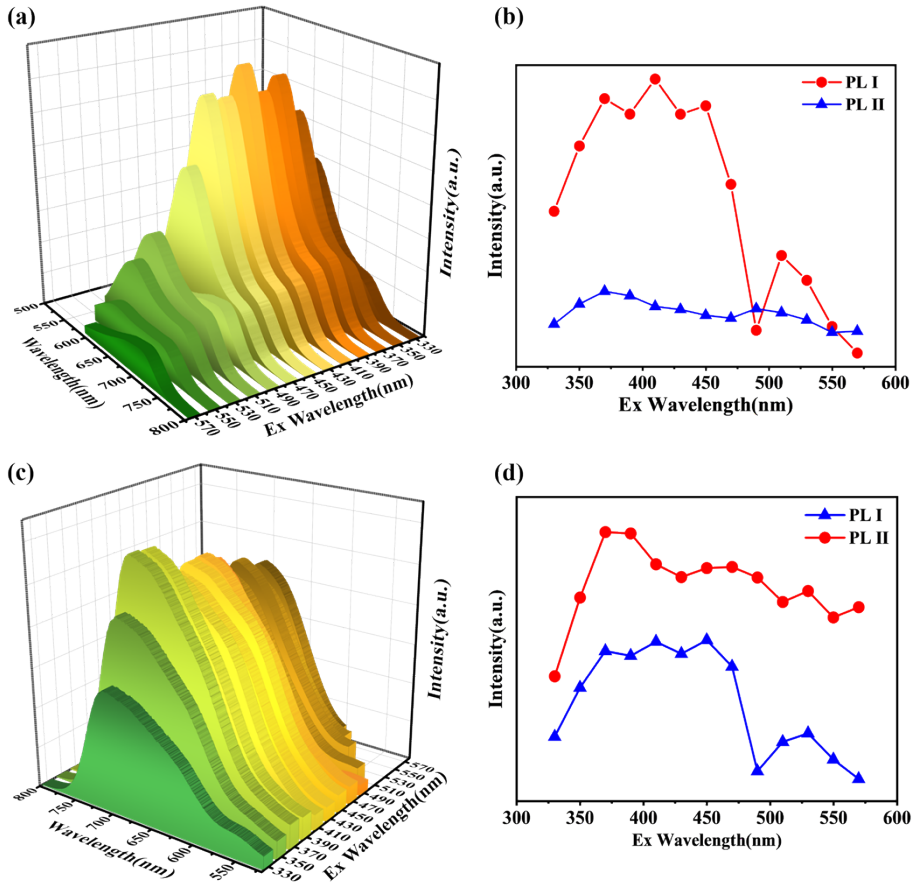


**Figure S13.** (a-b) The change trends of PL I and PL II of **$AuCu_{14}$-$CH_3$** under different excitations in $CH_2Cl_2$. (c-d) The change trends of PL I and PL II of **$AuCu_{14}$-$CH(CH_3)_2$** under different excitations in $CH_2Cl_2$.

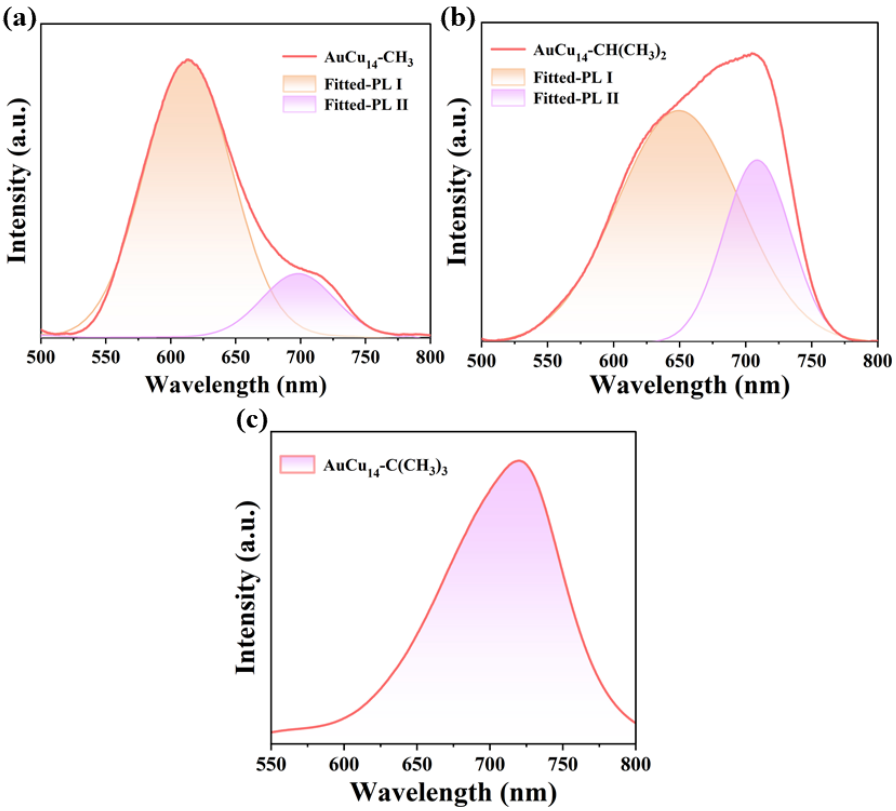


**Figure S14.** PL spectra of **$AuCu_{14}$-$CH_3$**, **$AuCu_{14}$-$CH(CH_3)_2$** and **$AuCu_{14}$-$C(CH_3)_3$** in DCM. Orange and purple areas represent the fitted PL I and PL II, respectively.

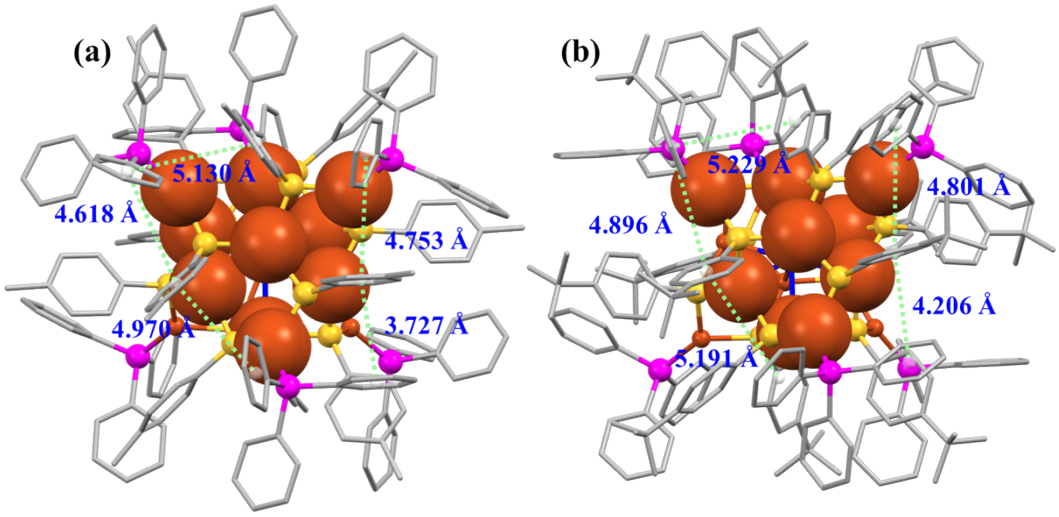


**Figure S15.** Overlay of (a) **$AuCu_{14}$-$CH_3$** and (b) **$AuCu_{14}$-$C(CH_3)_3$** SCXRD structures capturing the orientation differences of carbon tails.

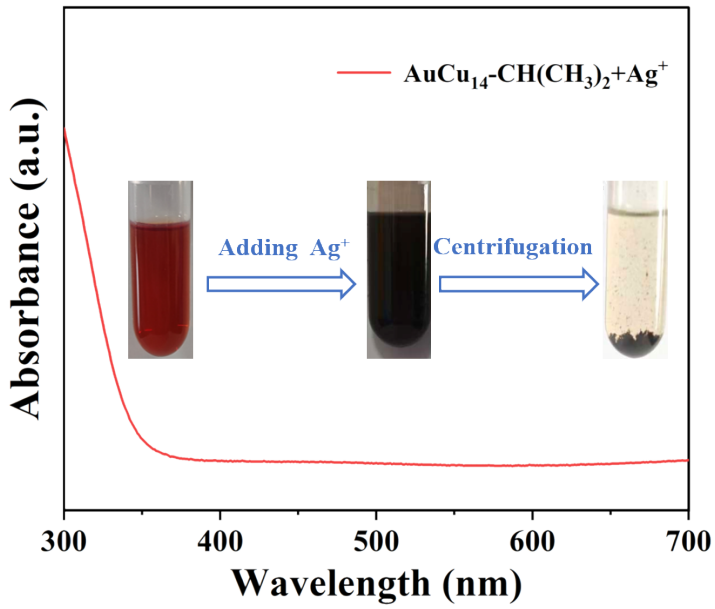


**Figure S16.** UV-vis absorption spectra of the supernatant after the addition of $Ag^+$ ion into **$AuCu_{14}$-$CH(CH_3)_2$** solution (inset: photographs of the reaction system).

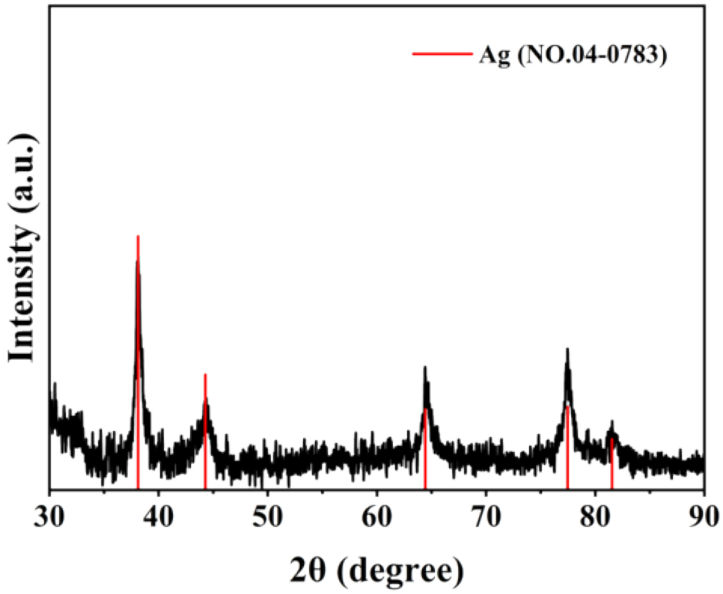


**Figure S17.** XRD spectrum of the precipitation after the addition of $Ag^+$ ion into **$AuCu_{14}$-$CH(CH_3)_2$** solution.

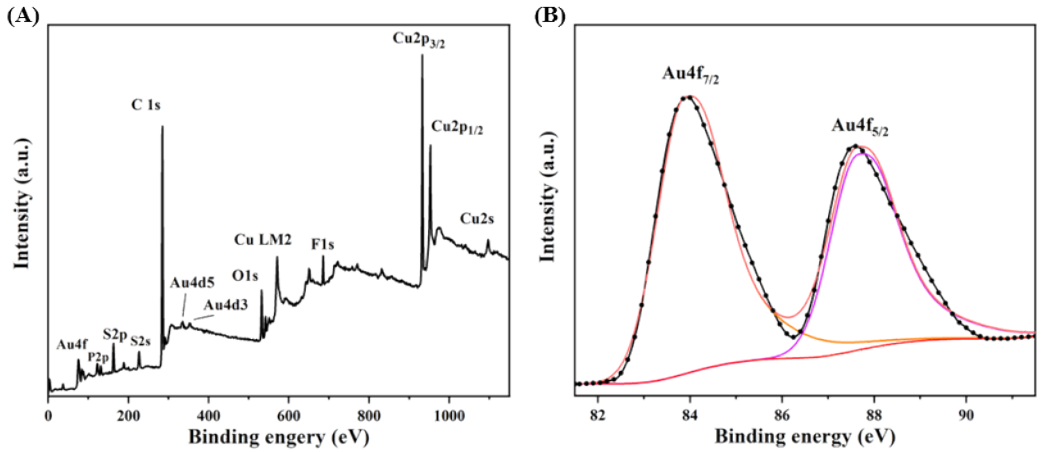

**Figure S18.** (A) The X-ray photoelectron spectroscopy (XPS) spectrum of crystalline **$AuCu_{14}$**; (B) the high-resolution of Au 4f part.

**Table S1.** Experimental single crystal X-ray data.

| **Identification code** | **$AuCu_{14}$-$CH_3$** | **$AuCu_{14}$-$CH(CH_3)_2$** | **$AuCu_{14}$-$C(CH_3)_3$** |
|---|---|---|---|
| Empirical formula | $C_{192}H_{174}Au_{0.6}Cu_{14}F_{5.4}P_6S_{12}Sb_{0.9}$[a] | $C_{216}H_{216}AuCu_{14}P_6S_{12}$ | $C_{228}H_{246}AuCu_{14}F_6P_6S_{12}Sb$ |
| Formula weight | 4271.76 | 4251.23 | 4879.05 |
| Temperature /K | 120 | 120.15 | 120 |
| Crystal system | Triclinic | monoclinic | Triclinic |
| Space group | P-1 | $P2_1/n$ | P-1 |
| a /Å | 16.5353(2) | 19.4553(2) | 18.9192(3) |
| b /Å | 16.7733(2) | 27.6070(2) | 20.0872(3) |
| c /Å | 19.1444(3) | 21.0119(3) | 21.2779(2) |
| α /° | 110.9310(10) | 90 | 65.5700(10) |
| β /° | 109.6290(10) | 95.8050(10) | 76.1360(10) |
| γ /° | 98.0240(10) | 90 | 62.742(2) |
| Volume /Å$^3$ | 4463.14(11) | 11227.7(3) | 6532.17(19) |
| Z | 1 | 2 | 1 |
| $\rho_{calc}$ g/cm$^3$ | 1.589 | 1.257 | 1.240 |
| μ /mm$^{-1}$ | 5.981 | 4.379 | 4.632 |
| F(000) | 2156.0 | 4126.0 | 2486.0 |
| Radiation | CuKα (λ = 1.54186 Å) | CuKα (λ = 1.54184Å) | CuKα (λ = 1.54184Å) |
| 2 θ range for data collection/° | 5.438 to 132 | 5.576 to 129.996 | 5.264 to 140 |
| Index ranges | -19≤ h ≤ 15, -19 ≤ k ≤ 19, -22 ≤ l ≤ 22 | -22≤ h ≤17, -32≤ k ≤ 28, -24 ≤ l ≤ 23 | -22≤ h ≤23, -24≤ k ≤ 24, -25 ≤ l ≤ 25 |
| Reflections collected | 55053 | 70984 | 93303 |
| Independent reflections | 15529 [$R_{int}$ = 0.0662, $R_{sigma}$ = 0.0475] | 18938 [$R_{int}$ = 0.0631, $R_{sigma}$ = 0.0468] | 24657 [$R_{int}$ = 0.0748, $R_{sigma}$ = 0.0505] |
| Data/restraints/parameters | 15529/30/874 | 18938/4655/1099 | 24657/124/1298 |
| Goodness-of-fit on F$^2$ | 1.077 | 1.025 | 1.008 |
| Final R indexes [I>=2σ (I)][b] | $R_1$ = 0.0748, $wR_2$ = 0.1997 | $R_1$ = 0.0952, $wR_2$ = 0.2644 | $R_1$ = 0.0544, $wR_2$ = 0.1484 |
| Final R indexes [all data][b] | $R_1$ = 0.0786, $wR_2$ = 0.2015 | $R_1$ = 0.0992, $wR_2$ = 0.2690 | $R_1$ = 0.0573, $wR_2$ = 0.1507 |
| CCDC | 2366812 | 2496270 | 1940446 |

[a] Formula is given based on single-crystal X-ray data.
[b] $R_1 = \Sigma||F_o| - |F_c||/ \Sigma|F_o|$, $wR_2 = \{ \Sigma[w(F_o^2-F_c^2)^2]/ \Sigma[w(F_o^2)^2]\}^{½}$

**Table S2.** Average bond length (Å) in **$AuCu_{14}$-$C(CH_3)_3$**, **$AuCu_{14}$-$CH(CH_3)_2$** and **$AuCu_{14}$-$CH_3$**.

| | Au-Cu | Cu-Cu | Cu-S |
|---|---|---|---|
| **$AuCu_{14}$-$C(CH_3)_3$** | 2.669 | 3.084 | 2.270 |
| **$AuCu_{14}$-$CH(CH_3)_2$** | 2.679 | 3.096 | 2.272 |
| **$AuCu_{14}$-$CH_3$** | 2.706 | 3.127 | 2.278 |

**Table S3.** The primary bond length of **$AuCu_{14}$-$CH_3$**.

| Bond | Length(Å) | Bond | Length(Å) |
|---|---|---|---|
| Au1-Cu2 | 2.778 | Au1-Cu4 | 2.791 |
| Au1-Cu5 | 2.594 | Au1-Cu6 | 2.661 |
| Au1-Cu8 | 2.778 | Au1-Cu10 | 2.791 |
| Au1-Cu12 | 2.594 | Au1-Cu14 | 2.661 |
| Cu2-Cu4 | 3.229 | Cu2-Cu5 | 3.008 |
| Cu2-Cu6 | 3.132 | Cu4-Cu12 | 3.085 |

| | | | |
|---|---|---|---|
| Cu4-Cu13 | 3.295 | Cu5-Cu11 | 3.085 |
| Cu5-Cu13 | 3.017 | Cu6-Cu11 | 3.295 |
| Cu6-Cu12 | 3.017 | Cu9-Cu11 | 3.229 |
| Cu9-Cu12 | 3.008 | Cu9-Cu13 | 3.132 |
| Cu2-S1 | 2.293 | Cu2-S5 | 2.274 |
| Cu2-S6 | 2.279 | Cu4-S2 | 2.284 |
| Cu4-S4 | 2.273 | Cu4-S6 | 2.293 |
| Cu5-S2 | 2.307 | Cu5-S3 | 2.287 |
| Cu5-S5 | 2.295 | Cu6-S1 | 2.264 |
| Cu6-S3 | 2.290 | Cu6-S4 | 2.306 |
| Cu9-S7 | 2.293 | Cu9-S11 | 2.274 |
| Cu9-S12 | 2.279 | Cu11-S8 | 2.284 |
| Cu11-S10 | 2.273 | Cu11-S12 | 2.293 |
| Cu12-S8 | 2.307 | Cu12-S9 | 2.287 |
| Cu12-S11 | 2.295 | Cu13-S7 | 2.264 |
| Cu13-S9 | 2.290 | Cu13-S10 | 2.306 |
| S3-Cu1 | 2.257 | S6-Cu1 | 2.286 |
| S4-Cu3 | 2.250 | S5-Cu3 | 2.263 |
| S1-Cu7 | 2.266 | S2-Cu7 | 2.250 |
| S9-Cu8 | 2.257 | S12-Cu8 | 2.286 |
| S10-Cu10 | 2.250 | S11-Cu10 | 2.263 |
| S7-Cu14 | 2.266 | S8-Cu14 | 2.250 |

**Table S4.** The primary bond length of **$AuCu_{14}$-$CH(CH_3)_2$**.

| Bond | Length(Å) | Bond | Length(Å) |
|---|---|---|---|
| Au1-Cu1 | 2.729 | Au1-Cu3 | 2.721 |
| Au1-Cu5 | 2.706 | Au1-Cu7 | 2.561 |
| Au1-Cu8 | 2.729 | Au1-Cu10 | 2.721 |
| Au1-Cu12 | 2.706 | Au1-Cu14 | 2.561 |
| Cu1-Cu7 | 3.012 | Cu3-Cu7 | 2.974 |
| Cu5-Cu7 | 2.949 | Cu5-Cu10 | 3.217 |
| Cu5-Cu8 | 3.217 | Cu3-Cu12 | 3.203 |
| Cu3-Cu8 | 3.225 | Cu1-Cu12 | 3.225 |
| Cu1-Cu10 | 3.203 | Cu12-Cu14 | 2.949 |
| Cu10-Cu14 | 2.973 | Cu8-Cu14 | 3.013 |
| Cu1-S2 | 2.289 | Cu1-S4 | 2.289 |
| Cu1-S5 | 2.266 | Cu3-S1 | 2.292 |
| Cu3-S3 | 2.275 | Cu3-S4 | 2.292 |
| Cu5-S1 | 2.295 | Cu5-S2 | 2.285 |
| Cu5-S6 | 2.270 | Cu7-S3 | 2.276 |
| Cu7-S5 | 2.279 | Cu7-S6 | 2.286 |
| Cu8-S8 | 2.289 | Cu8-S10 | 2.289 |

| | | | |
|---|---|---|---|
| Cu8-S11 | 2.266 | Cu10-S7 | 2.292 |
| Cu10-S9 | 2.275 | Cu10-S10 | 2.292 |
| Cu12-S7 | 2.295 | Cu12-S8 | 2.285 |
| Cu12-S12 | 2.270 | Cu14-S9 | 2.276 |
| Cu14-S11 | 2.279 | Cu14-S12 | 2.286 |
| S1-Cu2 | 2.256 | S5-Cu2 | 2.238 |
| S2-Cu4 | 2.261 | S3-Cu4 | 2.255 |
| S4-Cu6 | 2.263 | S6-Cu6 | 2.246 |
| S7-Cu9 | 2.256 | S11-Cu9 | 2.238 |
| S8-Cu11 | 2.261 | S9-Cu11 | 2.255 |
| S10-Cu13 | 2.263 | S12-Cu13 | 2.246 |

**Table S5.** The primary bond length of **$AuCu_{14}$-$C(CH_3)_3$**.

| Bond | Length(Å) | Bond | Length(Å) |
|---|---|---|---|
| Au1-Cu2 | 2.555 | Au1-Cu3 | 2.743 |
| Au1-Cu5 | 2.707 | Au1-Cu7 | 2.670 |
| Au1-Cu9 | 2.555 | Au1-Cu10 | 2.743 |
| Au1-Cu12 | 2.707 | Au1-Cu14 | 2.670 |
| Cu2-Cu3 | 3.005 | Cu2-Cu5 | 2.914 |
| Cu2-Cu7 | 3.033 | Cu3-Cu12 | 3.337 |
| Cu3-Cu14 | 3.122 | Cu5-Cu10 | 3.337 |
| Cu5-Cu14 | 3.092 | Cu7-Cu10 | 3.122 |
| Cu7-Cu12 | 3.092 | Cu9-Cu10 | 3.005 |
| Cu9-Cu12 | 2.914 | Cu9-Cu14 | 3.033 |
| Cu2-S2 | 2.281 | Cu2-S3 | 2.281 |
| Cu2-S5 | 2.281 | Cu3-S1 | 2.275 |
| Cu3-S2 | 2.273 | Cu3-S6 | 2.273 |
| Cu5-S4 | 2.299 | Cu5-S5 | 2.258 |
| Cu5-S6 | 2.281 | Cu7-S1 | 2.302 |
| Cu7-S3 | 2.285 | Cu7-S4 | 2.275 |
| Cu9-S8 | 2.281 | Cu9-S9 | 2.281 |
| Cu9-S11 | 2.281 | Cu10-S7 | 2.275 |
| Cu10-S8 | 2.273 | Cu10-S12 | 2.273 |
| Cu12-S10 | 2.299 | Cu12-S11 | 2.258 |
| Cu12-S12 | 2.281 | Cu14-S7 | 2.302 |
| Cu14-S9 | 2.285 | Cu14-S10 | 2.275 |
| S2-Cu1 | 2.247 | S4-Cu1 | 2.240 |
| S1-Cu4 | 2.267 | S5-Cu4 | 2.246 |
| S3-Cu6 | 2.247 | S6-Cu6 | 2.247 |
| S8-Cu8 | 2.247 | S10-Cu8 | 2.240 |
| S7-Cu11 | 2.267 | S11-Cu11 | 2.246 |
| S9-Cu13 | 2.247 | S12-Cu13 | 2.247 |

**Table S6.** Photophysical data of three $AuCu_{14}$ nanoclusters in $CH_2Cl_2$ under ambient conditions.。

| Solution phase | $AuCu_{14}$-$C(CH_3)_3$ | Solution phase | $AuCu_{14}$-$CH(CH_3)_2$ | $AuCu_{14}$-$CH_3$ |
|---|---|---|---|---|
| $\Phi_{PL}$(%) | 4.13 | $\Phi_{PL}$(%) | 5.37 | 5.76 |
| PL $\tau_{ave}$ (μs) | 3.3 | PL I $\tau_{ave}$ (ns) | 175.2 | 109.9 |
| | | PL II $\tau_{ave}$ (μs) | 3.0 | 2.5 |
| PL $k_r$ ($s^{-1}$) | $1.4\times10^4$ | PL I $k_r$ ($s^{-1}$) | $2.1\times10^5$ | $4.2\times10^5$ |
| | | PL I $k_{nr}$ ($s^{-1}$) | $5.5\times10^6$ | $8.7\times10^6$ |
| PL $k_{nr}$ ($s^{-1}$) | $2.9\times10^5$ | PL II $k_r$ ($s^{-1}$) | $5.4\times10^3$ | $4.4\times10^3$ |
| | | PL II $k_{nr}$ ($s^{-1}$) | $3.3\times10^5$ | $4.0\times10^5$ |

## Reference


[1] T. N. Hooper, C. P. Butts, M. Green, M. F. Haddow, J. E. McGrady, C. A. Russell, *Chem. Eur. J.* **2009**, 15, 12196-12200.
[2] K. J. Kilpin, R. Horvath, G. B. Jameson, S. G. Telfer, K. C. Gordon, J. D. Crowley, *Organometallics* **2010**, 29, 6186-6195.
[3] P. Gao, J. Du, W. J. Hong, M. Z. Wu, Y. Feng, Y. J. Ding and M. Z. Zhu, *Small Struct.* **2024**, 6, 2400397.
[4] O.V. Dolomanov, L.J. Bourhis, R.J Gildea, J.A.K. Howard, H. Puschmann, *J. Appl. Cryst.* **2009**, 42, 339-341.
[5] G.M. Sheldrick, *Acta Cryst.* **2015**, A71, 3-8.
[6] G. M. Sheldrick, *Acta Cryst.* **2008**, A64, 112-122.